



Cite this: *New J. Chem.*, 2020, 44, 17854

Supramolecular assembly of calix[4]resorcinarenes and chitosan for the design of drug nanocontainers with selective effects on diseased cells†

Ruslan Kashapov,^{id}*^a Yuliya Razuvayeva,^a Albina Ziganshina,^{id}^a Tatiana Sergeeva,^{id}^a Nadezda Kashapova,^a Anastasiia Sapunova,^{id}^a Alexandra Voloshina,^a Irek Nizameev,^{id}^a Vadim Salnikov^{bc} and Lucia Zakharova^{id}^a

In this paper, the spontaneous formation of nanoparticles through supramolecular interactions between chitosan and sulfonated calix[4]resorcinarenes was demonstrated. A set of physical–chemical methods were used to determine the ratio of components favorable for the formation of mixed aggregates, the size and the morphology of these aggregates formed in water solutions. The encapsulating and biological properties of the resulting chitosan–calix[4]resorcinarene compositions were studied. The stability of the obtained compositions with the encapsulated substrate was investigated over time. The cytotoxicity study showed their selective effect on the tumor cell line. The design pathway described here can be applied for the formation of various functional drug delivery systems comprising chitosan and macrocycles.

Received 29th April 2020,
Accepted 14th September 2020

DOI: 10.1039/d0nj02163f

rsc.li/njc

1. Introduction

Nanosized particles for the delivery of therapeutic compounds to pathogenic cells and tissues have become extremely popular in modern medicine due to their ability to penetrate across various biological barriers. The formation of these particles using noncovalent self-assembly is very challenging, since supramolecular assemblies provide great opportunities in the development of biomimetic systems.¹ Supramolecular amphiphiles (superamphiphiles) containing different macrocycles can be used for the design of drug delivery systems.^{2,3} The synthesis of nanoparticles without covalent modification significantly reduces the time and eliminates the presence of by-products in the system. In this regard, the nanoformulations formed by non-covalent interactions between synthetic compounds and natural biomaterials are widely developed.

Chitosan is an aminopolysaccharide extensively used as a natural material in the preparation of supramolecular polymeric nanoparticles. At neutral and alkaline pH, chitosan has free amino groups that can be protonated under acidic conditions, which opens up the possibility of ionic crosslinking when interacting with counterions. It is known that insoluble

stoichiometric and soluble non-stoichiometric polyelectrolyte complexes are formed as a result of the reaction between oppositely charged polyelectrolytes in water solutions.^{4,5} The macromolecules of polyelectrolytes in these complexes are retained by the cooperative interactions of predominantly ionic and hydrogen bonds, as well as the forces of dispersion interactions arising between the individual links of macromolecules.

Using the electrostatic complexation technique chitosan is also mixed with various macrocycles, such as sulfonated cyclodextrins,^{6–12} porphyrins^{13–16} and calix[4]arene.¹⁷ In these studies, chitosan and macrocycle form ion counterparts capable of self-assembling into nanoparticles with enhanced functional properties. The mixed aggregates of chitosan with porphyrins are used to create films and photosensitizers, while chitosan with cyclodextrins forms various types of aggregates for drug delivery. In the case of cyclodextrins, the formation of large aggregates (gels⁷ and platelets¹⁴) and small vesicular particles is possible. The vesicles based on cyclodextrins and chitosan are able to encapsulate both hydrophilic drugs in the inner core⁹ and hydrophobic substrates in the cyclodextrin cavity.⁶

A literature review has shown that there is only one example of using calix[4]arene derivatives in the creation of supramolecular polymeric vesicles with chitosan.¹⁷ These vesicles have the same dimensions and functions as those of aggregates of chitosan with cyclodextrins. Moreover, there are no works devoted to the design of mixed aggregates between resorcinarenes and chitosan. However one can expect additional stabilization of electrostatic interactions between sulfonated resorcinarenes and

^a Arbuzov Institute of Organic and Physical Chemistry, FRC Kazan Scientific Center of RAS, Arbuzov Str. 8, 420088 Kazan, Russia. E-mail: kashapov@iopc.ru

^b Kazan Institute of Biochemistry and Biophysics, FRC Kazan Scientific Center of RAS, Lobachevsky Str. 2/31, 420111 Kazan, Russia

^c Kazan Federal University, Kremlyovskaya Str. 18, 420008 Kazan, Russia

† Electronic supplementary information (ESI) available. See DOI: 10.1039/d0nj02163f

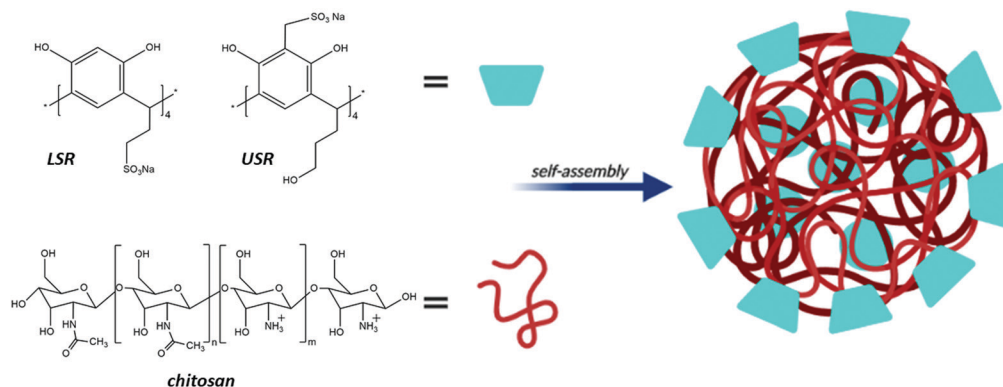


Fig. 1 Chemical formulas of sulfonated calix[4]resorcinarenes and chitosan and construction of supramolecular nanoparticles based on them.

chitosan due to intermolecular hydrogen bonds between their hydroxyl groups. Therefore, in the present study the rigid macrocycles, calix[4]resorcinarenes with sulfonate groups on the upper (USR) and lower (LSR) rim (Fig. 1), were chosen to stabilize mixed assemblies with more flexible chitosan. The presence of anionic sulfonate groups in the calix[4]resorcinarene structure would contribute to electrostatic interactions with chitosan protonated in acidic medium, and the hydroxyl groups of macrocycles may additionally stabilize the complex formed due to hydrogen bonds.

2. Materials and methods

2.1. Materials

Chitosan (50 000–190 000 Da based on viscosity, 75–85% deacetylated, Sigma-Aldrich), rhodamine B (Acros Organics, ≥98%) and doxorubicin hydrochloride (DOX) (Alfa Aesar, 99.7%) were used as received. Sample solutions were prepared in deionized water (18.2 MΩ) obtained from a Millipore Direct-Q 5 UV water purification system.

USR was synthesized from calix[4]resorcinarene¹⁸ as described in ref. 19. Briefly, 3.45 g (27.4 mmol) of Na₂SO₃ and 0.823 g (27.4 mmol) of paraform were mixed in 5 mL of water at 80 °C until completely dissolved. A suspension of calix[4]resorcinarene¹⁸ (2 g, 2.74 mmol) in 30 mL of ethanol was added in small portions. The suspension was stirred at 80 °C for 6 h. The precipitate was filtered and washed with ethanol. Then the precipitate was dissolved in water and the pH of the aqueous solution was adjusted to 5–6 by the addition of hydrochloric acid. The solution was dialyzed (3 × 30 minutes, 30 mL vs. 600 mL) using a dialysis bag with a MWCO of 1 kDa. After removal of the solvent, the oil was triturated in ethanol until a precipitate formed. Yield 3.14 g (96%). Mp > 350 °C. ¹H NMR spectrum (D₂O): 7.21 (4H, CH_{arom}), 4.50 (4H, CH), 4.29 (8H, CH₂-SO₃), 3.65 (CH₂-OH), 2.21 (8H, CH₂); 1.57 (8H, CH₂). ¹³C NMR spectrum (D₂O): 152, 125, 122, 108, 62, 48, 34, 30, 29. IR spectrum (cm⁻¹): 3390, 2939, 2871, 1608, 1473, 1414, 1213, 1150, 1041, 979, 900, 800, 778, 760, 664, 630, 545, 497. MALDI-TOF mass spectrum for C₄₄H₅₂O₂₄S₄⁴⁻: calculated: 1093; found: 1163 (C₄₄H₅₂O₂₄S₄⁴⁻ + 3Na⁺), 1208 (C₄₄H₅₂O₂₄S₄⁴⁻ + 5Na⁺). Elemental analysis for C₄₄H₅₂Na₄O₂₄S₄: calculated: C, 44.59; H, 4.42; Na, 7.76; S, 10.82; found: C, 44.26; H,

4.68; Na, 7.89; S, 10.89. The structure of USR is proved by ¹H NMR, ¹³C NMR and IR (Fig. S1–S3, ESI†).

LSR was synthesized according to the literature procedure described in ref. 20. Briefly, 2.0 g (10 mmol) of 2-(2-bromoethyl)-1,3-dioxane and 2.5 g (20 mmol) of Na₂SO₃ in 10 mL of water were stirred at 100 °C for 24 h. Then 2.0 g (18 mmol) of resorcinol in 20 mL of ethanol and 3 mL of concentrated hydrochloric acid were added. The mixture was stirred in an argon atmosphere at 100 °C for 24 h. The solvent was removed under reduced pressure. The residue was dissolved in 30 mL of water and dialyzed (3 × 30 minutes, 30 mL vs. 600 mL) using a dialysis bag with a MWCO of 1 kDa. The solvent was removed and the residue was recrystallized from ethanol. Yield 1 g (40%). Mp > 350 °C. ¹H NMR spectrum (D₂O): 6.94 (4H, CH_{arom}), 6.38 (4H, CH_{arom}), 4.55 (4H, CH), 2.92 (8H, CH₂-SO₃), 2.44 (8H, CH₂). ¹³C NMR spectrum (D₂O): 152, 126, 123, 103, 50, 34, 29. IR spectrum (cm⁻¹): 3450, 2970, 2950, 1620, 1510, 1175, 1050. MALDI-TOF mass spectrum for C₃₆H₃₆O₂₀S₄⁴⁻: calculated: 916; found: 1000.5 [M + 2Na + K], 1008.0 [M + 4Na]. Elemental analysis for C₃₆H₃₆Na₄O₂₀S₄ × 10H₂O: calculated: C, 36.36; H, 4.75; Na, 7.73; S, 10.79; found: C, 36.02; H, 4.43; Na, 8.21; S, 10.30. The structure of LSR is proved by ¹H NMR, ¹³C NMR and IR (Fig. S4–S6, ESI†).

2.2. Fabrication of nanoparticles

Aqueous solution of quaternized chitosan (QC) was prepared in a flask followed by the addition of solid polymer powder in acetate buffer placed in an ultrasonic bath until the polymer was completely dissolved to obtain a solution with a concentration of 1 mg mL⁻¹. Next, a fixed amount of the macrocycle was dissolved in the prepared QC solution to obtain compositions with different macrocycle concentrations.

2.3. Encapsulation of substrates (rhodamine B and DOX)

Rhodamine B- and DOX-loaded nanoparticles were prepared as follows: a specified amount of substrate was added to 5 mL solutions of 0.5 mM macrocycle–1 mg mL⁻¹ QC. In this mixture before dialysis the concentration of rhodamine B was 0.02 mM, and the concentrations of DOX were 0.02 and 0.1 mM. Subsequently, the unloaded substrate was removed from the obtained solution using the dialysis bag diffusion method (molecular weight cutoff 2000 Da) in 250 mL of distilled water

within 24 h. The amount of loaded substrate was determined spectrophotometrically by means of a calibration curve (Fig. S7, ESI†). The encapsulation efficiency (EE%) value was calculated using the following equation:

$$EE\% = (m_{\text{substrate-loaded}}/m_{\text{substrate}}) \times 100$$

where $m_{\text{substrate-loaded}}$ and $m_{\text{substrate}}$ are the mass of the substrate encapsulated in macrocycle-QC aggregates and the mass of the substrate added to macrocycle-QC aggregates, respectively.

The amount of DOX released into external water was tracked using fluorimetry. After 24 h of dialysis the fluorescence intensity remained virtually unchanged (Fig. S8, ESI†), so we decided to release the unencapsulated drug using dialysis for 24 h. The DOX loading efficiency was calculated by the following equation:

$$\text{loading efficiency (\%)} = (m_{\text{DOX-loaded}}/m_{\text{NPs}}) \times 100$$

where $m_{\text{DOX-loaded}}$ and m_{NPs} are the mass of DOX encapsulated in macrocycle-QC aggregates and the mass of DOX-loaded macrocycle-QC aggregates, respectively.

2.4. Characterization of particles

The diameters of the aggregates were determined by dynamic light scattering on a Zetasizer Nano instrument (Malvern Instruments, UK). The source of laser radiation was a He-Ne gas laser with a power of 4 mW and a wavelength of 632.8 nm. The same instrument with laser Doppler velocimetry and phase analysis light scattering was used for zeta potential measurements. The temperature of the scattering cell was controlled at 25 °C. Measurements were repeated at least five times. All scattering data were processed using the Malvern Zetasizer Software.

For IR experiments the solutions containing 2 mM calix[4]resorcinarenes and 1 mg mL⁻¹ QC were prepared in acetate buffer. The resulting precipitates in these solutions were dried. The IR spectra of solid samples of calixarenes, chitosan and mixed systems were recorded in KBr tablets in the range of 4000–400 cm⁻¹ with a resolution of 4 cm⁻¹ using a Bruker Vector 22 spectrometer.

Analysis of samples was carried out using a Hitachi HT7700 transmission electron microscope. Sample preparation was performed in the following way: 5 µL of the suspension was placed on a Formvar/carbon coated 3 mm copper grid (400 mesh), and drying was performed at room temperature for 24 h. Analysis was carried out at an accelerating voltage of 100 kV in TEM mode.

2.5. *In vitro* DOX release

In vitro DOX release experiments were conducted using a dialysis procedure. An aqueous solution (3 mL) of macrocycle-QC-DOX system was added in a dialysis bag (molecular weight cutoff 2000 Da). Then the dialysis bag was immersed in 200 mL of phosphate buffer solution (pH 7.4) or acetate buffer (pH 5.5). The dialysis system was kept at 37 °C with gentle stirring. At predefined time intervals, the amount of DOX in the

medium of macrocycle-QC was quantified in terms of its UV-vis absorbance at 481 nm.

2.6. Cell viability evaluation

Cytotoxic effects of the test compounds on human cancer and normal cells were estimated by means of the multifunctional Cytell Cell Imaging system (GE Health Care Life Science, Sweden) using the Cell Viability Bio App, which precisely counts the number of cells and evaluates their viability from fluorescence intensity. Two fluorescent dyes that selectively penetrate the cell membranes and fluoresce at different wavelengths were used in the experiments. DAPI (Sigma-Aldrich) is able to penetrate intact membranes of living cells and stains nuclei blue and the propidium iodide dye (Sigma-Aldrich) penetrates only dead cells with damaged membranes, staining them yellow. IC50 was calculated using the online IC50 calculator Quest Graph™ IC50 Calculator. The M-HeLa clone 11 human, epithelioid cervical carcinoma, a strain of HeLa, a clone of M-HeLa from the Type Culture Collection of the Institute of Cytology (Russian Academy of Sciences) and the Chang liver cell line (Human liver cells) from N. F. Gamaleya Research Center of Epidemiology and Microbiology were used in the experiments. The cells were cultured in a standard Eagle's nutrient medium manufactured at the Chumakov Institute of Poliomyelitis and Virus Encephalitis (PanEco company) and supplemented with 10% fetal calf serum and 1% nonessential amino acids. The cells were plated into a 96-well plate (Eppendorf) at a density of 1×10^5 cells per mL in 150 µL of medium per well, and cultured in a CO₂ incubator at 37 °C. Twenty-four h after seeding the cells into wells, 150 µL of the compound under study at a preset dilution was added to each well. The dilutions of the compounds were prepared immediately in nutrient media; 5% DMSO that does not induce inhibition of cells at this concentration was added for better solubility. The experiments were repeated three times. Intact cells cultured in parallel with experimental cells were used as a control.

2.7. Cellular uptake study of calixarene-QC particles loaded with DOX

Cellular uptake of free DOX and DOX-loaded compositions was analyzed by flow cytometry. Flow cytometry was used to set up statistics on the uptake of drug by human cancer and normal cells. Untreated cells were used as negative control. M-HeLa and Chang liver cells were seeded in 24-well plates at 1×10^6 cells per well and were incubated for 24 h. Then cells were cultivated with solutions of free DOX and DOX-loaded aggregates of USR- and LSR-QC for 24 h. Concentrations of DOX in the tested solutions were 0.00125 and 0.0025 mM. Fresh culture medium without test-compounds was added to control cells. After treatment, cells were rinsed three times with phosphate buffered saline (PBS) to remove any free test-compounds. The cells were then trypsinized and resuspended in fresh PBS with 10% fetal bovine serum. Cell suspensions were analyzed using Guava easy Cyte (Merck, USA).

2.8. Fluorescence microscopy

Chang liver cells in an amount of 1×10^5 cells per well in a final volume of 2 mL were seeded in 6-well plates with coverslips at the bottom of each well. After 24 h of incubation, free DOX and DOX-USR-QC were added to the wells and cultured for 24 h in a CO₂ incubator. Then, after treatment with free DOX and DOX-USR-chitosan, Chang liver cells were fixed and stained with Hoechst 33342 (blue). Studies were performed using a Nikon Eclipse Ci-S fluorescence microscope (Nikon, Japan) at a magnification of 1000 \times .

3. Results and discussion

Self-assembly and characterization of macrocycle-QC compositions

Two calix[4]resorcinarenes with different positions of the sulfonate groups were chosen for supramolecular assembly with QC in an aqueous solution. Since the amino groups of chitosan have a pK_a value of about 6.5, the stock polymer solution was prepared in acetate buffer with a pH of 5.5, which provides a cationic water-soluble form of the polymer capable of electrostatically interacting with oppositely charged macrocycles. The start of the self-assembly process based on the electrostatic complexation between macrocycles and QC was initially measured by optical transmittance at 450 nm. Fig. 2 shows the dependence of absorption at this wavelength on the macrocycle concentration in an aqueous system with a constant concentration of QC (1 mg mL^{-1}). The addition of macrocycles up to a concentration of 0.5 mM slightly increases the absorption value, and from 0.5 mM the absorption strongly increases with increasing concentration, indicating the formation of large-sized supramolecular assemblies. Moreover, the optical density in the system with LSR increases faster than that in the system with USR, *i.e.* the mixed aggregation of QC with LSR is relatively higher than with USR. This phenomenon can probably be due to the fact that the hydroxyl groups on the lower rim of USR, which has a greater cross-sectional height than LSR, are remote

from the sulfonate groups and hydroxyl groups of the upper rim and interact with the polymer, making the mixed aggregates looser. Another possible reason for the higher affinity of QC for LSR may be the greater flexibility of its sulfoethyl group, in contrast to the sulfomethyl group of USR.

As can be seen from Fig. S9 (ESI[†]), the mixed macrocycle-QC solutions demonstrate a clear Tyndall effect, indicating the existence of abundant nanoparticles. Similar phenomena are not observed for solutions of free macrocycle and QC, showing that they cannot form nanoscale aggregates under the same concentrations. It is interesting to note that a more pronounced Tyndall effect is manifested for the mixed composition with LSR, which correlates well with turbidimetric data. The absorption measurements were carried out up to concentrations of 1.5 mM and 2 mM for LSR and USR, respectively, since the systems were unstable and precipitated at higher concentrations. The inflection obtained on these dependencies indicates the preferred ratio of components for mixed aggregation. The optimal concentration of both macrocycles for compaction of 1 mg mL^{-1} QC in an aqueous solution is 0.5 mM.

For a more detailed study of the effect of macrocycles on the QC aggregation behavior, the dynamic light scattering (DLS) method was used. The DLS shows a monomodal particle size distribution for single QC solution with large (510 nm) particles. This size of aggregates decreases with an increase of the content of calixarenes in the mixture with QC (Fig. S10a, ESI[†]). The first portion of the added macrocycles (0.5 mM) leads to a sharp decrease in the particle size to 170 nm (Fig. 3a). In this case, the formed aggregates were detected with a good correlation function, which indicates their spherical shape. Further addition of calixarenes leads to nonmonotonic changes in the hydrodynamic diameter (Fig. S10b, ESI[†]). Thus, the presence of USR and LSR in an aqueous solution of QC leads to a decrease in the size, which means that the linear QC molecule is compacted to form spherical structures. The driving force of polymer compaction is the electrostatic interaction of its positively charged amino groups with the sulfonate groups of macrocycles, which is confirmed by electrophoretic light scattering. The zeta-potential value of the mixed solution containing 0.5 mM macrocycle is positive (Fig. 3b). A significant decrease in the positive zeta-potential is observed with an increase of macrocycle concentration in the aqueous medium with a constant amount of QC (Fig. S11, ESI[†]).

The mixed solutions of 1 mg mL^{-1} QC with 0.5 mM LSR and 0.5 mM USR diluted by two orders of magnitude were characterized by transmission electron microscopy (TEM). TEM results show that the QC-macrocycle compositions form spherical aggregates with an average size of around 50 nm for the composition with USR (Fig. 4a) and around 70 nm for the composition with LSR (Fig. 4c). The presence of larger aggregates in LSR-QC solution correlates with greater absorption in the UV spectrum. Considering the fact that the formation of similar aggregates is not observed in individual solutions of macrocycles and polymer (Fig. S12, ESI[†]), the key factor of mixed aggregation between them is the presence of fragments in their structure, dissociating in water with the formation of oppositely charged ions.¹⁶

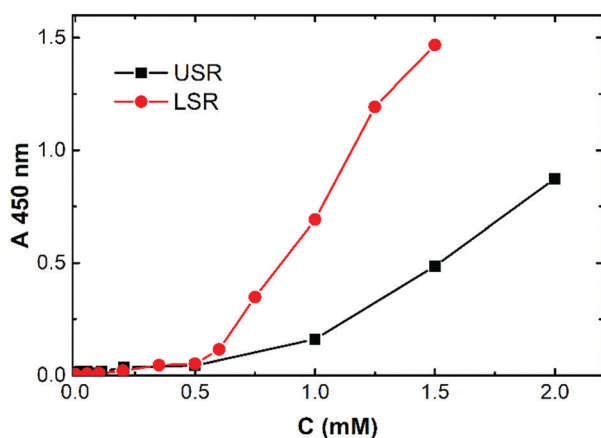


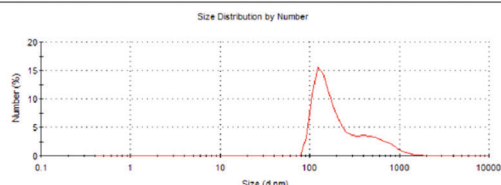
Fig. 2 Dependence of absorption intensity at 450 nm on the concentration of calix[4]resorcinarenes USR and LSR in aqueous solution with a fixed QC concentration of 1 mg mL^{-1} , acetate buffer pH 5.5.

a

0.5mM LSR - 1mg/ml QC

Z-Average (d.nm): 572.7	Peak 1: 165.0	% Number: 77.0	Width (nm): 63.09
Pdi: 0.424	Peak 2: 593.1	23.0	244.7
Intercept: 0.929	Peak 3: 0.000	0.0	0.000

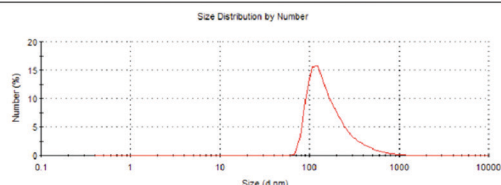
Result quality : Good



0.5mM USR - 1mg/ml QC

Z-Average (d.nm): 286.0	Peak 1: 177.5	% Number: 100.0	Width (nm): 129.8
Pdi: 0.424	Peak 2: 0.000	0.0	0.000
Intercept: 0.936	Peak 3: 0.000	0.0	0.000

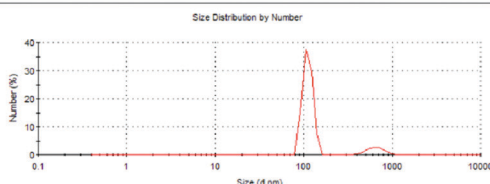
Result quality : Good



0.5mM LSR - 1mg/ml QC - DOX

Z-Average (d.nm): 552.6	Peak 1: 662.0	% Number: 10.4	Width (nm): 141.9
Pdi: 0.422	Peak 2: 111.8	89.6	14.06
Intercept: 0.945	Peak 3: 0.000	0.0	0.000

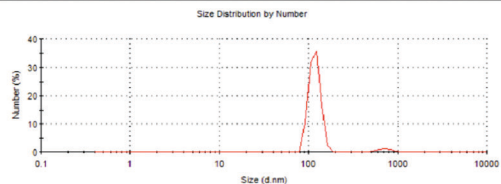
Result quality : Refer to quality report



0.5mM USR - 1mg/ml QC - DOX

Z-Average (d.nm): 339.7	Peak 1: 741.9	% Number: 3.5	Width (nm): 132.1
Pdi: 0.542	Peak 2: 117.8	96.5	16.72
Intercept: 0.945	Peak 3: 0.000	0.0	0.000

Result quality : Good

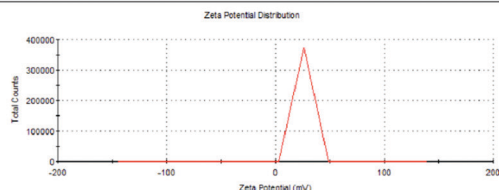


b

0.5mM LSR - 1mg/ml QC

Zeta Potential (mV): 25.9	Mean (mV): 25.9	Area (%): 100.0	Width (mV): 8.07
Zeta Deviation (mV): 8.07	Peak 1: 0.00	0.0	0.00
Conductivity (mS/cm): 7.03	Peak 2: 0.00	0.0	0.00
	Peak 3: 0.00	0.0	0.00

Result quality : Good



0.5mM USR - 1mg/ml QC

Zeta Potential (mV): 28.3	Mean (mV): 28.3	Area (%): 100.0	Width (mV): 10.2
Zeta Deviation (mV): 10.2	Peak 1: 0.00	0.0	0.00
Conductivity (mS/cm): 6.86	Peak 2: 0.00	0.0	0.00
	Peak 3: 0.00	0.0	0.00

Result quality : Good

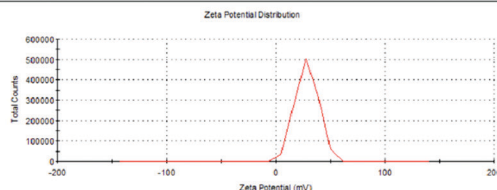


Fig. 3 (a) Particle size distributions for binary calix[4]resorcinarene–QC and triple calix[4]resorcinarene–QC–DOX systems, 25 °C, (b) zeta-potential for binary calix[4]resorcinarene–QC systems, 25 °C.

In order to verify bond formation between macrocycles and QC, FT-IR spectroscopy was used (Fig. 5). The peaks corresponding to -NH_2 and -OH groups²¹ were shifted from 3443 cm^{-1} (bulk chitosan) to 3435 cm^{-1} (USR–QC) and 3430 cm^{-1} (LSR–QC). The wider bands for mixed systems indicate that amine and hydroxyl groups in QC molecules form hydrogen bonds with macrocycles.^{22,23} The intensity of these bands corresponding to O–H and N–H vibrations for chitosan is certainly increased, which is related with the presence of OH groups in the macrocycle molecules. Compared to bulk chitosan, the vibrations corresponding to the I amide band of C=O (*N*-acetylamino groups) and N–H bending of the primary amine were shifted from 1655 cm^{-1} to 1639 cm^{-1} (USR–QC) and 1642 cm^{-1} (LSR–QC) and from 1561 cm^{-1} to 1560 cm^{-1}

(USR–QC) and 1557 cm^{-1} (LSR–QC), respectively. Differences between macrocycle and macrocycle–QC spectra may be observed at 1150 cm^{-1} and 1173 cm^{-1} bands attributed to S–O from USR and LSR, respectively. For the mixed composition of QC with macrocycles, these bands are shifted to 1154 cm^{-1} and 1188 cm^{-1} for USR–QC and LSR–QC, respectively, which once again proves the electrostatic interaction of macrocycles with QC and correlates with the data of electrophoretic light scattering.

We also attempted to investigate the complexation between macrocycles and chitosan using NMR spectroscopy. However, the individual solutions of macrocycles and the mixed systems were prepared not in acetate buffer, but in deuterated water acidified to pH 3.3. The choice of such a lower pH environment is related with the achievement of at least a small dissolution of

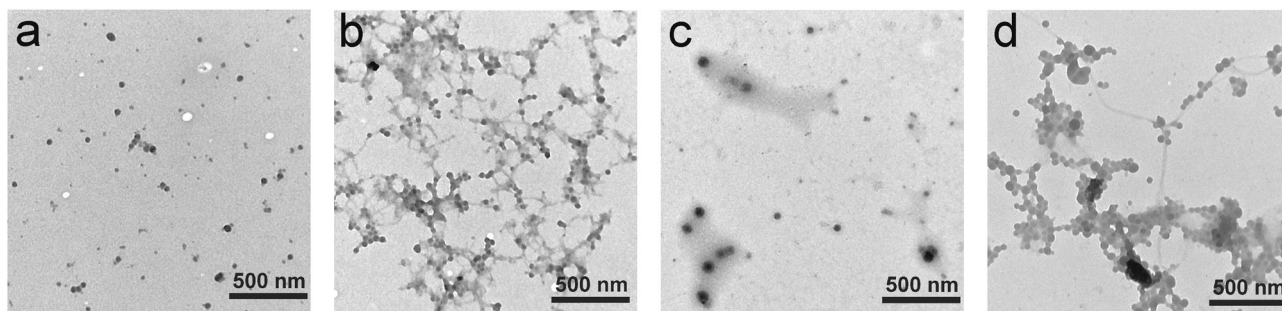


Fig. 4 TEM images of QC aqueous solution in the presence of USR (a) and LSR (c) and TEM images of USR-QC (b) and LSR-QC (d) solutions in the presence of DOX.

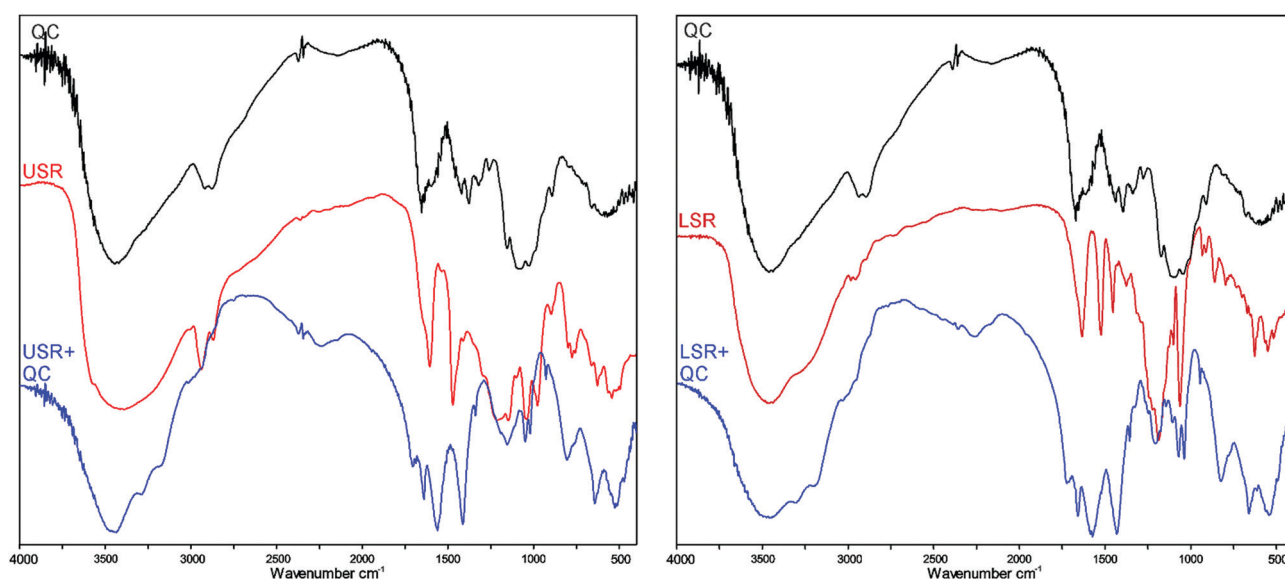


Fig. 5 FTIR spectra of chitosan, calix[4]resorcinarenes and mixed compositions.

chitosan. From the obtained ^1H NMR spectra of mixed systems for both macrocycles, a small change in chemical shifts for protons of the macrocycle lower rim is observed (Fig. S13 and S14, ESI †). Moreover, USR protons are shifted into the upfield region by 0.01–0.02 ppm after interaction with the polymer. In the case of LSR, para-aromatic and methylene protons near the bridge proton undergo a downfield change by the same chemical shift. Apparently, the degree of protonation of chitosan is not sufficiently large in these solutions, and we do not observe a change in chemical shifts near the sulfonate groups of macrocycles. Nevertheless, the obtained NMR spectroscopy data for a more hydrophobic chitosan than that formed in acetate buffer indicate a lack of inclusive interaction with the studied macrocycles.

Substrate loading and release

Further, the study of the encapsulation of a model hydrophilic probe, rhodamine B, into supramolecular aggregates by varying the macrocycle content in the mixed system with QC was carried out. As can be seen from the spectra presented in Fig. S15 (ESI †), the more the macrocycle concentration, the more rhodamine B is encapsulated in mixed aggregates with

QC. Rhodamine B encapsulated by the system with USR has one absorption band at 561 nm (Fig. S15a, ESI †), which is 6 nm different from the absorption maximum of free rhodamine B. In the case of the QC-LSR system, instead of one absorption band, two absorption bands are formed at 535 nm and 565 nm (Fig. S15b, ESI †). This type of spectrum is characteristic for J- and H-aggregates, which are usually formed at high concentrations of rhodamine B.²⁴ In both cases, the encapsulated rhodamine B produced absorption spectra different from the spectrum of free rhodamine B. Hence, the encapsulation efficiency was determined by the amount of substrate released through the dialysis membrane into external water. Despite the fact that a larger amount of macrocycle contributes to a larger amount of encapsulated substrate, the mixed systems with high concentrations of calixarenes are unstable in an aqueous medium and eventually precipitate. Therefore, the values of encapsulation efficiency (EE%) of rhodamine B were determined in stable mixed solutions with 0.5 mM calixarene and amounted to 100% for LSR and 29% for USR (Fig. S16, ESI †).

A similar difference in EE% was observed when studying the binding of a hydrophilic anticancer drug, doxorubicin

hydrochloride (DOX). As in the case of rhodamine B, we observed a high efficiency of DOX encapsulation in the 0.5 mM LSR-1 mg mL⁻¹ QC (EE% of 98%) system and low (almost half) encapsulation in the 0.5 mM USR-1 mg mL⁻¹ QC system (EE% of 51%) (Fig. S16, ESI[†]). These EE% values were obtained with the addition of 0.02 mM DOX and correspond to 0.0196 mM and 0.0102 mM of encapsulated drug for mixed systems with LSR and USR, respectively. Discovering an almost complete encapsulation of DOX in the composition with LSR, we decided to increase the initial concentration of encapsulated DOX to 0.1 mM. Then, 43.2 ± 1.6% and 19.8 ± 3.2% of initial amount of DOX were encapsulated by mixed systems with LSR and USR, respectively (Fig. 6a and b). These EE% values correspond to the concentrations 0.04 and 0.016 mM of DOX in ternary compositions with LSR and USR, respectively. According to UV-vis absorption spectra, the DOX loading efficiency values for LSR-QC and USR-QC compositions were calculated to be 4.41% and 1.54%, respectively. The reason for the high encapsulating ability of the LSR-QC composition toward hydrophilic substrates is probably due to the ability of this system to form hydrogen bonds with the encapsulated substrate. The formation of hydrogen bonds between macrocycle-polymer complexes and drug was detected by IR spectroscopy for the ternary system (Fig. S17, ESI[†]). While there are no significant changes in the positions of the bands in the IR spectrum between USR-QC and DOX, the IR spectrum for LSR-QC-DOX shows a change in the region of hydrogen bonds (3600–3100 cm⁻¹).

After establishing that the macrocycle-QC system encapsulated DOX, the *in vitro* release study of DOX was performed in PBS with pH 7.4 and acetate buffer with pH 5.5. As can be seen from Fig. 6a and b, the release of encapsulated DOX is observed in an acidic medium (pH 5.5) for both macrocycles. Moreover, in the system with USR a significant portion of the drug is released after 5 h and practically does not change over the next 9 h. Meanwhile, the drug release from the system with LSR is observed gradually over 18 h. Probably, the more prolonged release of DOX from the LSR-QC system is related with the formation of additional bonds between the drug and the complex. It is interesting to note the different behavior of DOX release from mixed systems in a neutral environment (pH 7.4). An increase in the absorption intensity after the release of DOX from the composition with USR (red solid line) relative to the UV spectrum of the mixture with the originally encapsulated drug (black solid line) is probably related with the opalescence caused by acidification to pH 7.1 during dialysis (Fig. 6a). Therefore, the absorbance band of DOX is overlapped by the formed precipitate in the UV spectrum of this system. Although a decrease in the intensity of this band is observed over time, its shape clearly indicates that DOX is not released. A similar lack of drug release in a neutral environment is also observed in a mixed system with LSR. This result is particularly significant, since the supramolecular polymeric particles have higher stability in the systemic circulation at physiological pH and therefore, they must provide DOX release in the cancer tissues with acidic pH.

Subsequently, the stability of empty and DOX-loaded mixed macrocycle-QC aggregates was studied. We determined the

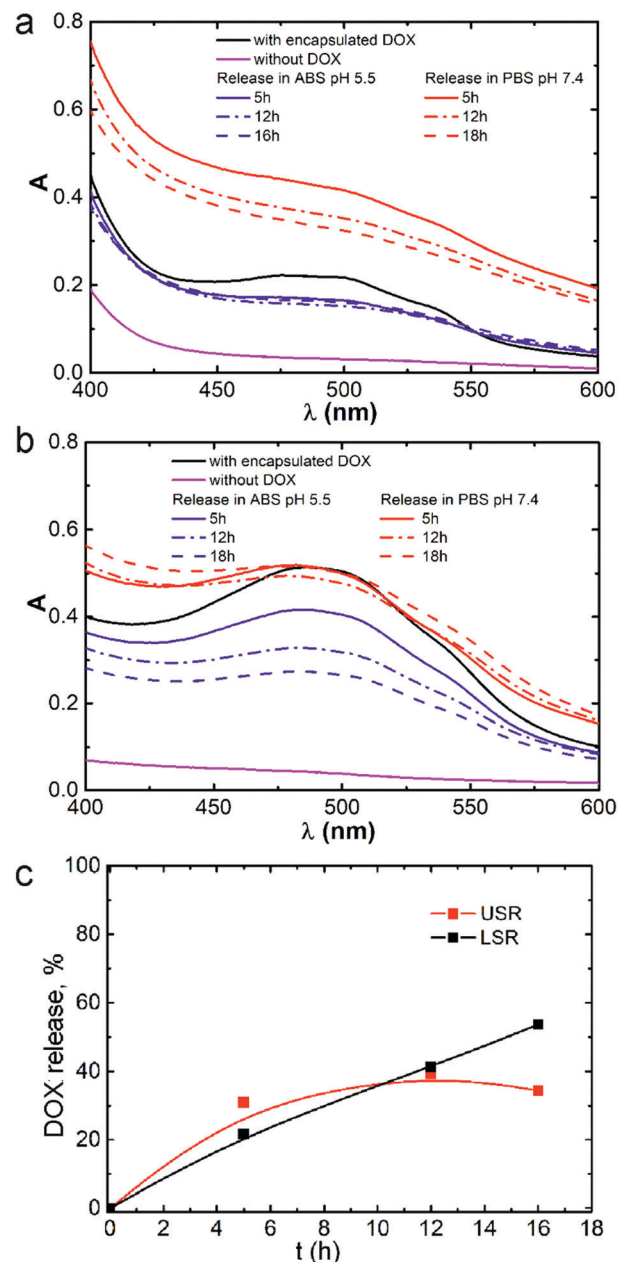


Fig. 6 UV spectra of 0.5 mM USR-1 mg mL⁻¹ QC (a) and 0.5 mM LSR-1 mg mL⁻¹ QC (b) in the absence and presence of encapsulated and released DOX in water (1 cm optical path length). (c) DOX release from 0.5 mM calix[4]resorcinarene-1 mg mL⁻¹ QC aggregates in acetate buffer solution (pH 5.5), 37 °C.

hydrodynamic diameters of these aggregates over time using DLS. From the obtained data presented in Fig. S18 (ESI[†]), it is clear that the empty aggregates based on USR are relatively stable, since they slightly change in size and remain at the level of 170 nm during 6 days. In contrast, the hydrodynamic diameter of aggregates with LSR changes non-monotonically, which probably indicates the dynamic nature of the aggregation process. It is worth noting that the encapsulation of DOX in macrocycle-QC aggregates can significantly affect their size. After encapsulation of DOX the structure of mixed aggregates is

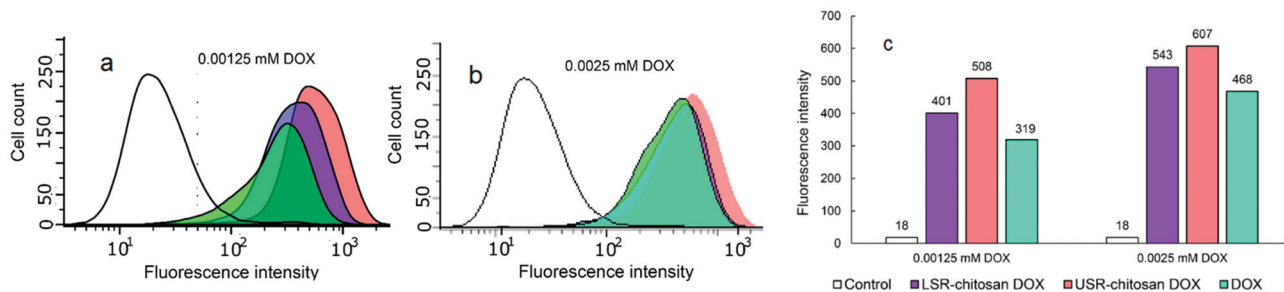


Fig. 7 Flow cytometry data of M-HeLa cells incubated with DOX-loaded QC aggregates with USR and LSR: (a) luminescence intensity of M-HeLa cells after 24 h incubation with LSR-QC-DOX and USR-QC-DOX ($C_{\text{DOX}} = 0.00125$ mM); (b) intensity of luminescence of M-HeLa cells after 24 h incubation with LSR-QC-DOX and USR-QC-DOX ($C_{\text{DOX}} = 0.0025$ mM); (c) the average fluorescence intensity from flow cytometry histograms is shown as a function of aggregate type and concentration.

preserved, but their diameter slightly changes and decreases, which was evident by DLS results and TEM images (Fig. 3 and 4). The particle size in USR-QC compositions with DOX decreases slightly to 110–120 nm (Fig. 3) and is stable at least for 8 days (Fig. S17, ESI[†]). At the same time, the hydrodynamic diameter of LSR-QC aggregates after DOX encapsulation significantly increases from 110 to 700 nm the following day. It is interesting that after DOX addition the agglomeration of particles and the appearance of fibers were observed on TEM images (Fig. 4b and d). It may be assumed that positively charged DOX partially displaced QC from aggregates and these polymer fibers bound particles. Probably, it is the same agglomerates that were detected as the second mode by the DLS method. Fig. 4b and d show an improvement of the aggregation in the macrocycle-QC-DOX systems, and, obviously, DOX promotes the formation of homogeneous particles. The chemical structure of DOX has two fragments: the aromatic part, which is solubilized in the hydrophobic region of the aggregates, and the aminosaccharide, which makes it soluble in water and can interact most likely with the charged groups of macrocycles. The crosslinking of the particles with each other can be due to the DOX binding effect or the high concentration and adhesion of the particles when the sample is applied to the surface and dried. Since the particles are charged, they can stick together not only with DOX, but also with the counterions. This binding is probably observed only on a surface, and in a dilute solution the aggregates are most likely to be in an individual state.

The high percentage of DOX encapsulation into aggregates with LSR is probably related with more dynamic aggregation behavior manifested in size growth. At the same time, the USR-QC system encapsulates a drug to a less extent due to higher stability. The stability of these DOX-loaded nanoparticles was also investigated in a physiological environment (PBS). The compositions 0.5 mM macrocycle–1 mg mL^{−1} QC were diluted twice with PBS and tested by DLS over time when comparing these compositions in acetate buffer solution. As can be seen from Fig. S19 (ESI[†]), the macrocycle-QC compositions are stable in PBS for three days. Further, the aggregates begin to grow, which leads to precipitation.

Cell uptake and cytotoxicity

Flow cytometry based on DOX fluorescence revealed cell absorption of DOX encapsulated in nanoparticles based on

QC and calixarenes (Fig. 7). The resulting mixed systems penetrate the cells, and DOX is more efficiently transferred due to USR, regardless of the drug concentration. Apparently, this contributes to the better activity of the USR-QC-DOX system against cancer cells (Table 1). It is worth noting that the particles of this system loaded with DOX have sizes less than 150 nm, which are optimal for the penetration of aggregates into the cell.

We further investigated the DOX location and distribution inside the Chang liver cells using fluorescence microscopy. The DNA intercalating dye, Hoechst 33342, was used to label cell nuclei (blue stain), while DOX was distributed in the cell nuclei with red fluorescence. Fig. S20 (ESI[†]) shows that the high fluorescence exhibited from free DOX and DOX-loaded USR-QC composition indicated that DOX was present in cells in significant quantities. These results revealed that a large amount of DOX was inside the nucleus and produced the purple fluorescent spots in the merged images. However, in the case of treatment by encapsulated DOX the fluorescence intensity is not so bright, which is probably due to the quenching of DOX emission due to its encapsulation in the aggregates.

Subsequent to establishing that macrocycle-QC-DOX systems penetrated the cancer cell, the cytotoxicity of single and mixed compositions on Chang liver and M-HeLa cells was evaluated *in vitro*. The unexpected toxicity of mixed formulations, as well as individual USR to healthy cells, is likely due to the presence of 29.6 mM acetic acid in acetate buffer. Moreover, the toxicity of mixed macrocycle-polymer systems in relation to healthy cells is higher than that to the cancer line. DOX loading into nanoparticles formed by calix[4]resorcinarenes and QC increases the effectiveness of the drug against cancer cells (Table 1). Recently, we also observed an increase in the cytotoxicity of DOX encapsulated in vesicles formed by calix[4]resorcinarene with glucamine fragments.²⁵ In other works, the vesicles formed by calixarene-based superamphiphiles did not affect DOX cytotoxicity to cancer cells and, at the same time, reduced damage to normal cells.^{26,27} In contrast to these previous works, our DOX-loaded calixarene-based systems with QC showed increased cytotoxicity with respect to tumor cells. It is interesting to note that in the present study of cytotoxicity a selective effect on the tumor cell line was achieved. The triple USR-QC-DOX system is less toxic to

Table 1 IC₅₀ for free LSR, USR, LSR-QC, USR-QC, DOX and DOX encapsulated in LSR-QC and USR-QC

	IC ₅₀	
	M-HeLa	Chang liver
LSR	> 250 μM	> 250 μM
USR	> 250 μM	132 \pm 9 μM
LSR-QC	170 μM –0.35 mg mL ^{−1}	70 μM –0.13 mg mL ^{−1}
USR-QC	200 μM –0.4 mg mL ^{−1}	50 μM –0.12 mg mL ^{−1}
DOX	5.2 \pm 0.4 μM	6.0 \pm 0.5 μM
LSR-QC-DOX	2.3 \pm 0.2 μM	4.2 \pm 0.3 μM
USR-QC-DOX	2.1 \pm 0.1 μM	6.3 \pm 0.4 μM

healthy liver cells. Thus, despite the fact that the USR-QC system encapsulates DOX almost less than half of the LSR-QC system, it is more stable in time, passes through the cell membrane to a greater extent, and is more selective towards diseased cells.

4. Conclusions

In summary, supramolecular interactions between sulfonated calix[4]resorcinarenes and quaternized chitosan lead to the spontaneous formation of supramolecular polymeric nanoparticles. The nanoparticles based on calix[4]resorcinarene with sulfonate groups on the upper rim encapsulate a drug practically less than half of those based on calix[4]resorcinarene bearing sulfonate groups on the lower rim, but they are more stable over time. The encapsulation of doxorubicin into polymeric nanoparticles based on the macrocycle with sulfonate groups on the upper rim increases drug activity toward tumor cells. The revealed pattern of the formation of nanoparticles, which have an encapsulating capacity toward hydrophilic substrates and a selective effect on diseased cells, is the most important step on the way of increasing the efficiency and rational use of anticancer drugs.

Conflicts of interest

There are no conflicts to declare.

Acknowledgements

The authors thank the Assigned Spectral-Analytical Center of FRC Kazan Scientific Center of RAS.

References

- M. Amit, S. Yuran, E. Gazit, M. Reches and N. Ashkenasy, Tailor-Made Functional Peptide Self-Assembling Nanostructures, *Adv. Mater.*, 2018, **30**, 1.
- X. Zhang and C. Wang, Supramolecular amphiphiles, *Chem. Soc. Rev.*, 2011, **40**, 94.
- M. Mingfang, X. Pengyao, L. Shangyang, C. Xiaoxiao, W. Bo and H. Aiyu, Advances of host-guest supramolecular vesicles and their properties in drug delivery, *Prog. Chem.*, 2014, **26**, 1317.
- V. A. Kabanov, Polyelectrolyte complexes in solution and in bulk, *Russ. Chem. Rev.*, 2005, **74**, 3.
- C. B. Rodell, J. E. Mealy and J. A. Burdick, Supramolecular Guest-Host Interactions for the Preparation of Biomedical Materials, *Bioconjugate Chem.*, 2015, **26**, 2279.
- Z. Wang and Y. Li, Raloxifene/SBE- β -CD inclusion complexes formulated into nanoparticles with chitosan to overcome the absorption barrier for bioavailability enhancement, *Pharmaceutics*, 2018, **10**, 76.
- D. K. Ho, A. Costa, C. De Rossi, C. De Souza Carvalho-Wodarz, B. Loretz and C. M. Lehr, Polysaccharide Submicrocarrier for Improved Pulmonary Delivery of Poorly Soluble Anti-infective Ciprofloxacin: Preparation, Characterization, and Influence of Size on Cellular Uptake, *Mol. Pharmacol.*, 2018, **15**, 1081.
- X. M. Chen, Y. Chen, X. F. Hou, X. Wu, B. H. Gu and Y. Liu, Sulfonato- β -Cyclodextrin Mediated Supramolecular Nanoparticle for Controlled Release of Berberine, *ACS Appl. Mater. Interfaces*, 2018, **10**, 24987.
- S. Duri and C. D. Tran, Supramolecular composite materials from cellulose, chitosan, and cyclodextrin: facile preparation and their selective inclusion complex formation with endocrine disruptors, *Langmuir*, 2013, **29**, 5037.
- N. A. Burns, M. C. Burroughs, H. Gracz, C. Q. Pritchard, A. H. Brozena, J. Willoughby and S. A. Khan, Cyclodextrin facilitated electrospun chitosan nanofibers, *RSC Adv.*, 2015, **5**, 7131.
- J. S. Yang and L. Yang, Preparation and application of cyclodextrin immobilized polysaccharides, *J. Mater. Chem. B*, 2013, **1**, 909.
- F. Carn, S. Nowak, I. Chaab, R. Diaz-Salmeron, M. Djabourov and K. Bouchemal, Autoassemblies of α -Cyclodextrin and Grafted Polysaccharides: Crystal Structure and Specific Properties of the Platelets, *J. Phys. Chem. B*, 2018, **122**, 6055.
- H. Jiang, W. Su, J. Hazel, J. T. Grant, V. V. Tsukruk, T. M. Cooper and T. J. Bunning, Electrostatic self-assembly of sulfonated C₆₀-porphyrin complexes on chitosan thin films, *Thin Solid Films*, 2000, **372**, 85.
- B. Liao, R. Liu and Y. Huang, Supramolecular Chiroptical Switch Based on Chitosan and Anionic Porphyrin Complex Film, *Polym. J.*, 2007, **39**, 1071.
- A. Synytsya, A. Synytsya, P. Blafková, J. Ederová, J. Spěváček, P. Slepíčka, V. Král and K. Volka, pH-controlled self-assembling of meso-tetrakis(4-sulfonatophenyl)porphyrin-chitosan complexes, *Biomacromolecules*, 2009, **10**, 1067.
- J. Zeng, W. Yang, D. Shi, X. Li, H. Zhang and M. Chen, Porphyrin Derivative Conjugated with Gold Nanoparticles for Dual-Modality Photodynamic and Photothermal Therapies *In Vitro*, *ACS Biomater. Sci. Eng.*, 2018, **4**, 963.
- S. Peng, K. Wang, D. S. Guo and Y. Liu, Supramolecular polymeric vesicles formed by *p*-sulfonatocalix[4]arene and chitosan with multistimuli responses, *Soft Matter*, 2015, **11**, 290.
- B. C. Gibb, R. G. Chapman and J. C. Sherman, Synthesis of Hydroxyl-Footed Cavitands, *J. Org. Chem.*, 1996, **61**, 1505.
- T. Y. Sergeeva, R. K. Mukhitova, I. R. Nizameev, M. K. Kadirov, P. D. Klypina, A. Y. Ziganshina and A. I. Konovalov,

- Closed polymer containers based on phenylboronic esters of resorcinarenes, *Beilstein J. Nanotechnol.*, 2018, **9**, 1594.
- 20 K. Kobayashi, Y. Asakawa, Y. Kato and Y. Aoyama, Complexation of Hydrophobic Sugars and Nucleosides in Water with Tetrasulfonate Derivatives of Resorcinol Cyclic Tetramer Having a Polyhydroxy Aromatic Cavity: Importance of Guest–Host CH– π Interaction, *J. Am. Chem. Soc.*, 1992, **114**, 10307.
 - 21 G. Lawrie, I. Keen, B. Drew, A. Chandler-Temple, L. Rintoul, P. Fredericks and L. Grøndahl, Interactions between alginate and chitosan biopolymers characterized using FTIR and XPS, *Biomacromolecules*, 2007, **8**, 2533.
 - 22 M. Tylman, K. Pieklarz, P. Owczarz, W. Maniukiewicz and Z. Modrzejewska, Structure of chitosan thermosensitive gels containing graphene oxide, *J. Mol. Struct.*, 2018, **1161**, 530.
 - 23 Y. Wu, X. Li, X. Shi, Y. Zhan, H. Tu, Y. Du, H. Deng and L. Jiang, Production of thick uniform-coating films containing rectorite on nanofibers through the use of an automated coating machine, *Colloids Surf., B*, 2017, **149**, 271.
 - 24 Q. Yuan, X. Zhang, Z. Wang, M. H. M. A. Shibraen, S. Yang and J. Xu, Dimerization of Rhodamine B in Alumina sol and corresponding dip-coated film, *Colloids Surf., A*, 2015, **486**, 139.
 - 25 R. R. Kashapov, Y. S. Razuvayeva, A. Y. Ziganshina, R. K. Mukhitova, A. S. Sapunova, A. D. Voloshina, I. R. Nizameev, M. K. Kadirov and L. Y. Zakharova, Design of *N*-Methyl-D-Glucamine-Based Resorcin[4]arene Nanoparticles for Enhanced Apoptosis Effects, *Mol. Pharmacol.*, 2020, **17**, 40.
 - 26 K. Wang, D. S. Guo and Y. Liu, Temperature-controlled supramolecular vesicles modulated by *p*-sulfonatocalix[5]arene with pyrene, *Chem. – Eur. J.*, 2010, **16**, 8006.
 - 27 K. Wang, D. S. Guo, X. Wang and Y. Liu, Multistimuli responsive supramolecular vesicles based on the recognition of *p*-sulfonatocalixarene and its controllable release of doxorubicin, *ACS Nano*, 2011, **5**, 2880.